JOURNAL OF AIRCRAFT
Vol. 32, No. 2, March–April 1995

Interpretation of Experimental High-Alpha Aerodynamics—Implications for Flight Prediction

Martin E. Beyers
Institute for Aerospace Research, Ottawa, Ontario K1A 0R6, Canada

Nomenclature

b = wingspan, or largest dimension
C = aerodynamic coefficient; with no superscript, in body axes system
C_{ij} = $\partial C_i/\partial(jl/2V)$, $i = l, m, n$; $j = q, q', \dot{\alpha}, \dot{\sigma}$ ($l = \bar{c}$); $j = p, \dot{\beta}, \dot{\phi}$ ($l = b$)
C_{ik} = $\partial C_i/\partial k$, $i = l, m, n$; $k = \alpha, \beta, \sigma$
C_l = rolling moment coefficient
C_m = pitching moment coefficient
C_n = yawing moment coefficient
C_p = static pressure coefficient
C_Y = side force coefficient
$\bar{c}$ = mean aerodynamic chord
d = body maximum diameter
h = height of test section
h_0 = model length
l = generalized reference length
M_∞ = freestream Mach number
p, p_s = local static pressure
p, q, r = body-axes angular velocities
q_∞ = freestream dynamic pressure
Re_l = Reynolds number based on l, $l = \bar{c}$, b, or d
S = reference area
V, V_∞ = freestream velocity
w = minimum dimension of test section
X, Y, Z = inertial axes system
X_f, Y_f, Z_f = flight coordinate system, Fig. 2
x, y, z = body axes system
α, β = angles of attack and sideslip
Δ = increment or amplitude
λ = inclination of rotation axis, Fig. 6
$\sigma, \hat{\phi}$ = total angle of attack and bank angle
φ_n = roll angle of nose tip
ψ, θ, ϕ = Euler angles
$\Omega, \dot{\phi}$ = coning rate, parameter $\Omega b/2V$ or $\bar{\Omega}$
$\bar{\omega}$ = reduced circular frequency, $\omega l/(2V)$, where $l = \bar{c}$ or b, as appropriate

Subscripts

a = apex
av = asymmetric vortices
c = rotation center, Fig. 2
s = support

Superscripts

$\dot{}$ = differentiation with respect to time
$\hat{}$, $'$ = aerodynamic axes system
*, $^-$ = composite derivative, Eq. (2)
$\sim$ = oscillatory condition

Introduction

WITH the increasing emphasis on high-α flight,[1] aerodynamic prediction technology has moved into the realm of dynamically separated flows and nonlinear responses, creating a new genre of experimental and analytical problems. In general, the physics of transient high-α unsteady phenomena cannot be described by existing theoretical methods, whether they be associated with rigid body motions,[2] natural flowfield unsteadiness,[3] or with vehicle deformation. Despite encouraging progress[4] numerical simulation of high-α aerodynamics is still a long way from maturity,[3,5] placing a heavy reliance on wind-tunnel experiments.[6] Wind-tunnel experiments are not without sources of error,[6] and the requirements for high-α experiments are quite challenging as the flowfields are intrinsically unsteady. Factors that influence the unsteady aerodynamic data include dynamic support interference,[7] unsteady wall interference,[8] and the more complex, test facility interference,[9,10] Reynolds number effects,[11] flow quality,[6] and effects of freestream turbulence.[12] Moreover, complete dynamic similitude may not be directly possible at subscale Reynolds numbers,[13] but appropriate experimental techniques in conjunction with numerical modeling can go a long way towards addressing the problem.

In flight, high-α conditions arise almost exclusively as a consequence of maneuvering or concomitant departure. Under such conditions the flow mechanisms may be dominated by kinematic or viscous fluid/motion coupling.[14] In the latter case, measurements on stationary wind-tunnel models have quite limited value, and experimental simulations should instead reflect the dynamic nature of the vehicle responses.[15] Both the test facility interference[9,10] and Reynolds number effects,[11] as well as possible effects of freestream turbulence, are inherently coupled with the body motion. Largely because of the ubiquitous viscous fluid/motion coupling, which is beyond present CFD capabilities,[16] the use of numerical methods to predict support and wall interference is currently restricted to static experiments.

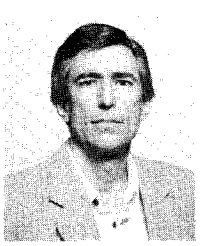

Martin Beyers is Head of the Aircraft Aerodynamics Group, Applied Aerodynamics Laboratory, at the National Research Council, Canada. He has conducted extensive research in high-alpha unsteady aerodynamics and free-flight dynamics, and is a coordinator of international activities related to maneuvering aerodynamics, including AGARD FDP Working Group 16 and TTCP HTP-5. He is an Associate Editor of the *Journal of Aircraft* and has served on the AIAA Technical Committees on Applied Aerodynamics and Atmospheric Flight Mechanics. He has a Ph.D. from Witwatersrand University, Johannesburg, South Africa, and has published over 70 papers.

Presented as Paper 94-0166 at the AIAA 32nd Aerospace Sciences Meeting and Exhibit, Reno, NV, Jan. 10–13, 1994; received Jan. 24, 1994; revision received June 24, 1994; accepted for publication June 30, 1994.

In this Paper, the experimental challenges are discussed in the broader context of the high-α unsteady aerodynamics, and of the requirements for flight predictions based on conventional mathematical models[17] or on hybrid flight simulations. In the absence of analytical models applicable to high-α maneuvers these requirements are illustrated through reference to free-flight experiments, which provide the analogue of actual flight. Existing wind-tunnel results are surveyed and the analyses of certain previous investigations extended to provide new insight into the mechanisms through which the coupling phenomena can restrict the usefulness of the experimental data.

Flight Mechanics Considerations

At present, flight prediction based on analytical models is not possible in the poststall domain. Nevertheless, simulations based on mathematical models that formulate the aerodynamic responses to arbitrary motions in terms of linear derivatives are in routine use.[17] At high α and high angular rates the underlying assumptions are violated with the onset of time-dependent, unsteady separation phenomena including aerodynamic bifurcations[18] and motion coupling. It is important to be able to determine when and how the analytical model breaks down, but this is difficult when the derivatives themselves are affected by the facility interference that prevails in the presence of separated flows.

Circumventing these difficulties researchers have concentrated on identifying and isolating the aerodynamic phenomena involved, in studies of specific single-degree-of-freedom (DOF) motions, such as the rapid pitch-up[19] and large-amplitude, high-rate roll oscillations.[20] In the near term, at least, flight predictions have to be based on interactive use of both numerical and experimental methods, resulting in hybrid 6-DOF simulations (Fig. 1). The ability to isolate the aerodynamic phenomena that define the flight simulation structure is critically dependent upon the understanding of the interference flow physics.

The present discussion is confined to rigid body motion, but has general relevance. Recognizing the importance of fluid/motion coupling, the question arises, what motion parameters should be simulated in dynamic tests? To illustrate the experimental requirements for 6-DOF simulation the angular motion is described in terms of the instantaneous rotation center and total angular velocity vector.

Planar Motion

For planar motion it may be sufficient to consider the pitch-oscillation and heave/plunge characteristic motions. In the presence of dynamically separated flows the aerodynamic reactions are nonlinear and the superposition principle does not hold. One way around this is to combine the two characteristic motions into a single motion. Rotation about the aircraft effective rotation center is equivalent to combined plunging and pitching about the center of mass (c.m.) (Fig. 2). Then the planar motion problem is reduced to a single-DOF problem, provided that the dynamic characteristics can be determined for this rotation center.

The problem is that in any given maneuver the effective center is not fixed and may have a complex locus in the x-z plane. This can be appreciated for the example of a missile model in free flight[15] (Fig. 3). During the first part of the trajectory the effective center x_c is fixed since the θ and Z_f motions are in phase quadrature, but in the subsequent trimmed motion the movement of the rotation center becomes nonlinear. Note that in Fig. 3 the rotation center is generally forward of the missile (h_0 = 0.151 m), a position that cannot easily be simulated in dynamic tests; only at the peak angle does the missile momentarily rotate about its c.m. The combination of rotary and translational motions determines the instantaneous velocity distribution along the vehicle; thus, the motion of the effective rotation center is associated with the unsteady

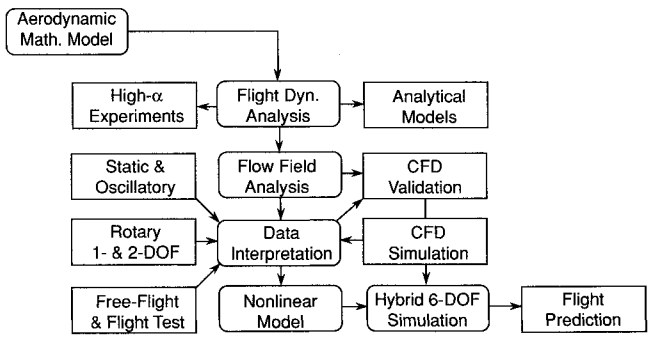

Fig. 1 Rationale for high-α flight prediction.

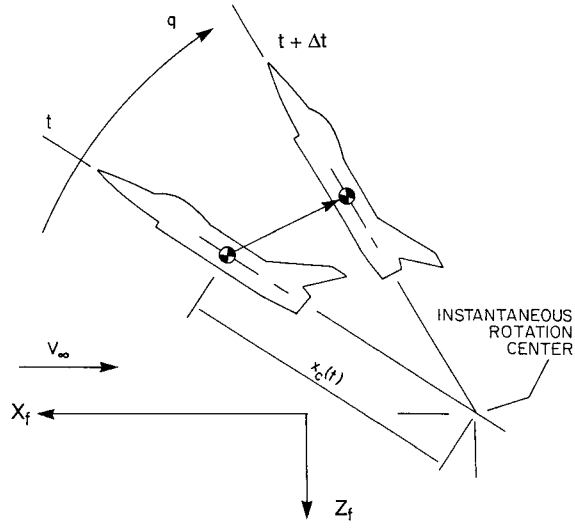

Fig. 2 Effective axis of rotation in flight.

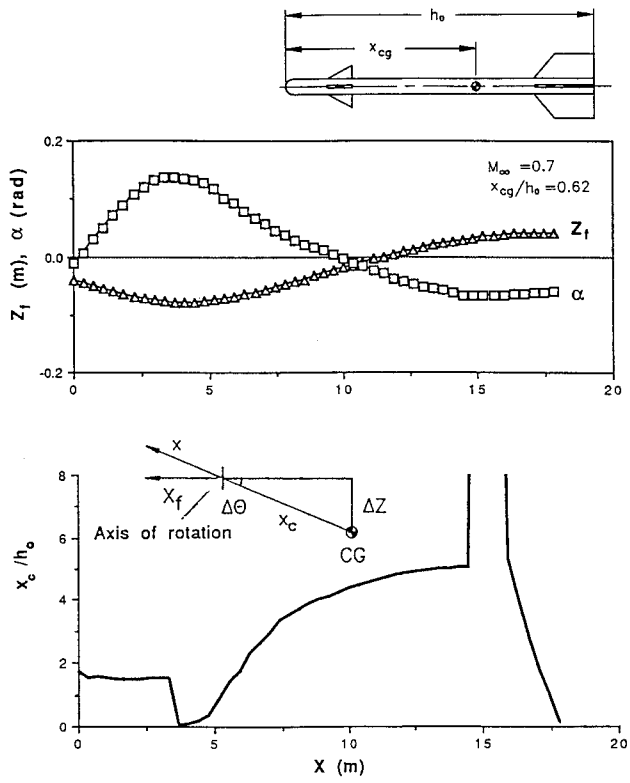

Fig. 3 Free-flight motion of destabilized missile model.[15]

flowfield evolution. Flowfield changes with pivot axis location can be dramatic, as observed in dynamic stall experiments.[21] Moreover, the dependence of dynamic derivatives on the axis location cannot easily be determined, partly because the dynamic support interference is dependent upon the rotation point.

The effects of the pitch rate are equally dramatic,[21] particularly when the motion is free of the single-DOF (forced-oscillation) constraint, since then it will govern the evolution of both flowfield and responses. The natural flow dynamics can be reproduced in free flight. For instance, the simulated wind-tunnel flight[22] of an aircraft-like model at $M_\infty = 0.6$ exhibits the high pitch rates typifying the Herbst maneuver[23] (Fig. 4). The initial pitch rate in Fig. 4 simulates 1.2 rad/s at full scale.

Nonplanar Motion

Unlike the case of the pitch-up motion, aircraft maneuvering is not, in general, kinematically simple. Figure 5 shows the $\alpha - \beta$, $\Omega - \alpha$, and $\lambda - \alpha$ plots for a free-flight spin test of a fighter aircraft.[24] During departure and recovery the loci of the motion variables are clearly arbitrary. At the spin equilibrium the motion degenerates into steady coning ($\lambda = 0$) (Fig. 6). For this mode rotary balance data are entirely appropriate and the kinematic analysis can be based quite simply on the balance of forces and moments in the spin.[25] However, such data may not be representative when the spin radius r_0 cannot be simulated (Fig. 6), because the velocity distribution on the aircraft forebody will not be correct. When the motion is unsteady, during maneuvering or departure, both the location r_0 and orientation λ of the spin axis have to be simulated. As before, the instantaneous 3-DOF motion is reduced to a 1-DOF motion.

Most fighters exhibit some degree of oscillatory spin, where more complex experimental[25-27] and analytical[28] methods are needed. Then the nonlinearity introduced by nonplanar aerodynamic coupling has to be incorporated in the equations of motion, in additon to kinematic coupling. The Tobak-Schiff[28] model specifies four characteristic motions from which the aerodynamic loads are synthesized. Formulated in the body axes system[28] and expressed in terms of aircraft motion variables[29] α, β, and V, for linear motion-rate dependence

$$C_k(t) = C_k(\infty, \alpha, \beta) + \frac{1}{\gamma}\frac{pl}{V} C_{k\phi}(\infty, \alpha, \beta) + (\dot{\alpha} - \dot{\beta}\tan\alpha\tan\beta)\frac{l}{V} C^*_{kq}(\alpha, \beta) - \frac{1}{\cos\alpha}\frac{\dot{\beta}l}{V} C^*_{kr}(\alpha, \beta) \quad (1)$$

where

$$C^*_{kp} = C_{kp} + C_{k\dot{\beta}}\sin\alpha - C_{k\dot{\alpha}}\cos\alpha\tan\beta$$
$$C^*_{kr} = C_{kr} - C_{k\dot{\beta}}\cos\alpha - C_{k\dot{\alpha}}\sin\alpha\tan\beta \quad (2)$$
$$C^*_{kq} = C_{kq} + C_{k\dot{\alpha}}, \qquad k = X, Y, Z, l, m, n$$

Linking the reactions in the aerodynamic and body-axes systems[28] yields an identity written here in the composite derivative notation[29] [Eq. (2)], where $\gamma = \cos\sigma$ and $\delta = \sin\sigma$

$$\hat{C}_{n\phi} - \gamma(C^*_{np}\cos\hat{\phi} + C^*_{mp}\sin\hat{\phi}) = \delta(C^*_{nr} + C^*_{mq} - \hat{C}_{m\dot{\alpha}}) \quad (3)$$

Test Facility Interference

An evaluation[30] of Eq. (3) for the standard dynamics model (SDM)[31-34] at $\beta = 0$ (Fig. 7) showed that the results are consistent at low α, but the correlation fails when the flowfield becomes substantially separated, at $\alpha \geq 20$ deg. This is precisely the point at which the applicability of the model formulated in terms of linear derivatives would be expected to break down. At the same time, with the onset of unsteady flow separation, inherently different motion coupling mechanisms come into play, resulting in fundamentally different facility interference effects[9] in the two cases. Since these effects are coupled it is neither possible to check the validity of the model nor to check the internal consistency of the dynamic derivatives in this domain. The correlation in terms of the identity in Eq. (3) constitutes a global check on the applicability of the model and dynamic data, and is, therefore, indicative of the degree of success that can be expected in a flight simulation under these conditions. Thus, to determine the domain of applicability of, and alleviate the uncertainty in flight predictions based on such models, it is necessary to correctly interpret the unsteady facility interference contributions.

The need to examine the interference contributions to the derivatives in Eq. (1) is especially important in the case of the cross-coupling derivatives. Sensitivity studies have shown that cross-coupling derivatives can play a significant role in

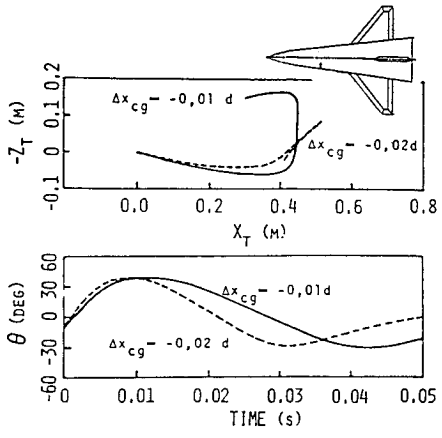

Fig. 4 Free-flight simulation of pitch-up maneuver.[22]

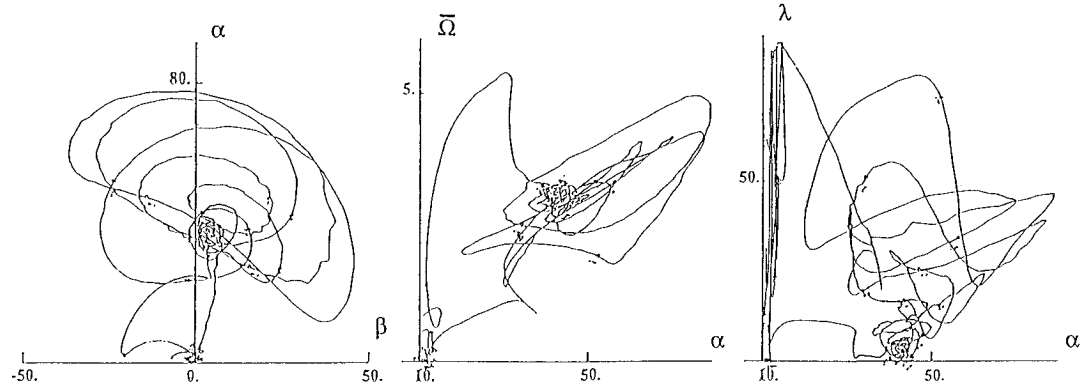

Fig. 5 Flight trajectory from spin test.[24]

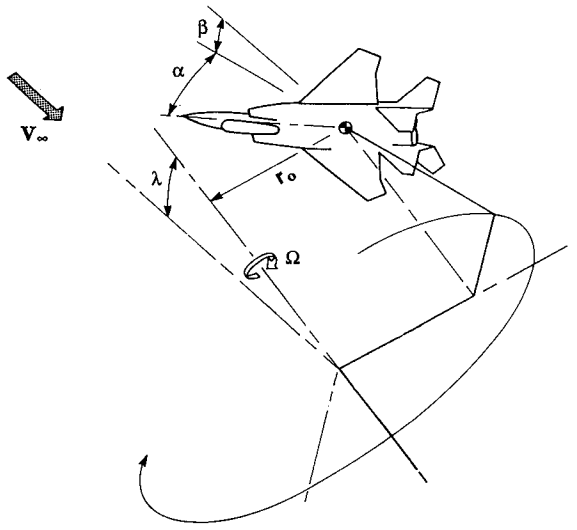

Fig. 6 Geometric parameters in aircraft spin.

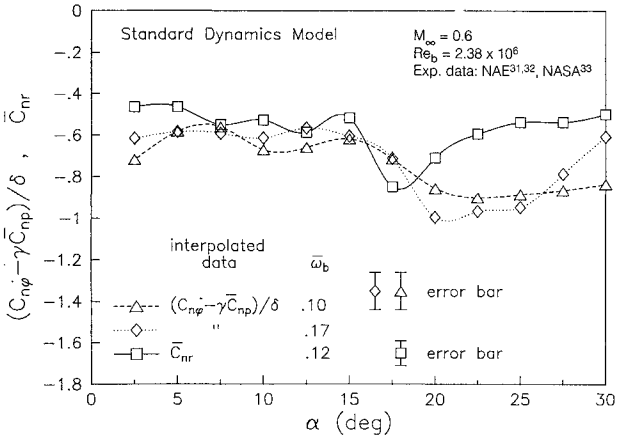

Fig. 7 Correlation of SDM data according to Eq. (3).[30]

nonplanar maneuvers.[35] However, since the presence of certain cross-coupling derivatives under symmetrical flight conditions is associated with the onset of asymmetrical flow separation, it is most important to establish whether these derivatives are applicable at all in the flight domain studied.

In the poststall domain nonlinear airloads determined experimentally for 1- or 2-DOF motions could be combined with numerical predictions to construct a hybrid nonlinear simulation (Fig. 1). Depending on the maneuver, this could demand complex 2-DOF experiments,[27] which would be subject to even more complex facility interference effects. Again, the uncertainty associated with such flight predictions could be rendered manageable only if the interference effects are understood. It is important to note that, although stability derivatives cannot represent nonlinear responses in the poststall regime, they do provide unsteady data that are useful for diagnostic purposes, containing the essential clues as to the role of viscous motion coupling and convective time lags in producing the facility interference.

Aerodynamic Prediction Methods

Impressive results have been obtained using Navier-Stokes[36] and Euler[5] methods as well as macro-aerodynamic modeling[37,38] to simulate the unsteady aerodynamics associated with forced oscillations. However, for a maneuvering flight vehicle, the 6-DOF rigid-body equations of motion and the equations governing the fluid flow are coupled, and have to be solved simultaneously. This has been accomplished, in principle, for the case of an autorotating flat plate.[39] The numerical methods

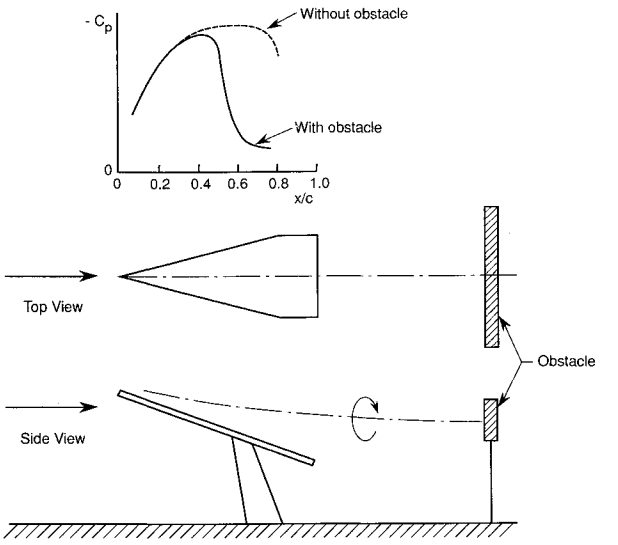

Fig. 8 Effect of obstacle on vortex burst on a 75-deg delta wing.[43]

have been successful when the vortex dynamics are kinematics-dominated. In contrast, when the fluid/motion coupling is a viscous process, occurring, e.g., through the so-called moving-wall effect,[40] the available analytical methods are quite restricted. For cases where fully turbulent flow can be assumed, numerical simulation complemented by experimental free-flight validation could yield useful results (Fig. 1). On the other hand, CFD simulation of unsteady phenomena occurring when the moving-wall effect is unsaturated[41] is not possible at present. CFD simulation is hampered by the absence of realistic transition models. Thus, analysis of unsteady facility interference on advanced aircraft models is beyond current CFD capabilities.

Ground Test Facility Interference

To understand the nature of the problem it is instructive to initially consider the facility-induced interference effects individually, and subsequently, take the coupling into account.

Support Interference Mechanisms

Support interference comes in many guises,[7] but in high-α experiments the effects generally fall into two categories, characterized by 1) strong interactions of the interference of a downstream obstacle on vortex flow/wake characteristics,[42] and 2) the more subtle effects of flowfield distortions.[9]

Strong Interactions

The direct effect of an obstacle positioned downstream of a model at high α was effectively demonstrated in Hummel's classic experiment.[43] Vortex breakdown was promoted significantly in the presence of the obstacle (Fig. 8). Another manifestation of such direct interference is found in asymmetry switching under conditions of asymmetrical vortex shedding from a slender forebody.[44] This is commonly associated with conventional support sectors or floor-to-roof struts. It is also very apparent in rotary balance data,[42] discussed below, but still a tractable problem by virtue of the steady nature of the disturbance. The interaction with the downstream support is complicated considerably when the motion of the model and/or support is unsteady. For oscillatory motion this is characterized by a convective time lag, in which case an analysis combining static and dynamic data to correct for support interference[45] may be possible.

Weak Interactions

Effects of the wake blockage of the support system causing weak interactions may be difficult to identify in static tests

when the strut is symmetrical, yet may produce significant unsteady effects. On the other hand, effects of similar magnitude produced by an asymmetric strut are more readily apparent.[46] Figure 9 is a composite of identical views from flow visualization experiments in the Institute for Aerospace Research (IAR) 2 × 3 m wind tunnel at $\sigma = 21.4$ deg ($\alpha = 19$ deg), with the SDM banked at $\hat{\phi} = 28.4$ and -28.4 deg ($\beta = \pm 10$ deg). The divergence of the symmetrically positioned smoke trails, and associated rotation of the plane of flow deflection,[46] is attributed to flowfield disturbances caused by the strut and the walls. The accompanying nonuniformities in the wall pressure distributions were equally pronounced, showing that the potential for effects on vortex breakdown exists in the range tested, 19 deg $\leq \alpha \leq$ 28 deg. Weak interaction of the type discussed here can be coupled with unsteady wall interference effects, in which case significant test facility interference may result.[9]

Unsteady Wall Interference

Unsteady wall interference[9] arises when disturbances originating at the model are reflected at the walls, or, alternatively, when disturbances generated at the walls are communicated to the model. The main sources of unsteady wall interference include pressure disturbances generated by the model, vortex-wake/wall interference at high α, the fluctuating pressure gradients due to unsteady separation in the diffuser or on the walls downstream of the support, and to the motion of the model and/or rig, and transverse acoustic interference.[47] If the tests are restricted to nonresonant frequencies, the latter can be dispensed with. The pressure fluctuations caused by model or support motion are superimposed on the test section static pressure gradients.[9,47]

Unsteady Interference Coupling

For the test installation shown in Fig. 9 it was demonstrated that both support and wall interference effects are present at high α.[46] Similar, but more severe, effects are evident in tests of the same SDM test configuration in a smaller, ventilated test section,[48] with $b/w = 0.6$. Pitch oscillations of the model at high incidence will be accompanied by fluctuating wake blockage with concomitant downstream fluctuations in the flowfield in which the strut/sting is immersed[9] (Fig. 10). The strut flow modulation will be communicated upstream to the model, resulting in either a strong or weak interaction with its separated flowfield.

This type of interaction has been referred to as "unsteady wind-tunnel interference"[9] or "ground facility interference."[10] The nature of the unsteady facility interference naturally depends on the test installation and motion characteristics, with quite different results in rotary and oscillatory tests.[9,10] Unsteady support/wall interference coupling appears to be the most common form of unsteady facility interference, but a variety of other mechanisms, such as the coupling between two unsteady wall inteference mechanisms, may also be present in high-α dynamic tests.[9]

Support Oscillation and Other Considerations

In dynamic testing support design is normally driven by both structural and aerodynamic requirements. When the rigidity criteria are paramount, rather bulky support struts will inevitably result. Symmetrical struts and sectors[49] (Fig. 11) are naturally unsuitable for yaw oscillation tests in general, and for pitch oscillation at finite sideslip angles, and an asymmetrical side-mount was designed[48] (Fig. 12). This avoided the strong-interaction interference as the vortex wake effectively cleared the A-frame strut at high α (Fig. 12). The resulting interference is a coupled support/wall interference[9] occurring at low α ($\alpha < 20$ deg).

The effects of support oscillation were studied analytically.[50-54] With the introduction of a complete set of equations for support oscillation correction[54] the design philosophy emphasizing rigidity was abandoned.[46] Instead, a larger measure of flexibility was tolerated in favor of improved strut/sting aerodynamics, introducing relatively slender stings.[46] What-

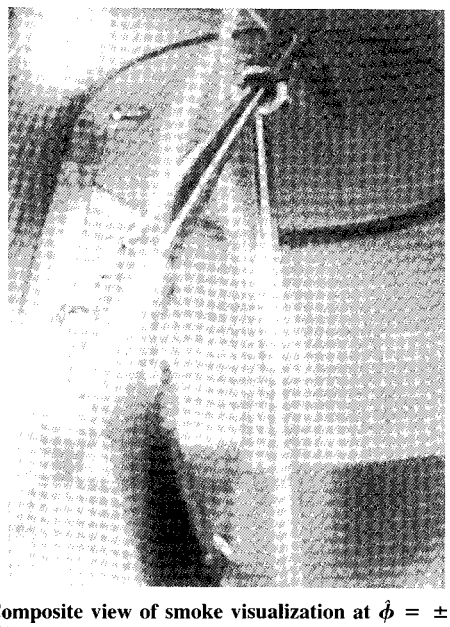

Fig. 9 Composite view of smoke visualization at $\hat{\phi} = \pm 28.4$, $\sigma = 21.4$ deg.[46]

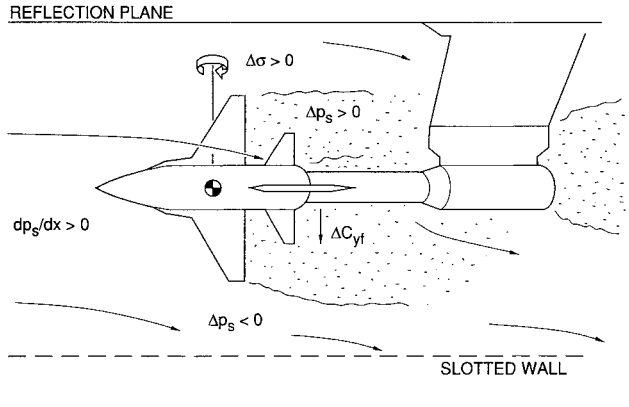

Fig. 10 Flowfield response to pitch change.[9]

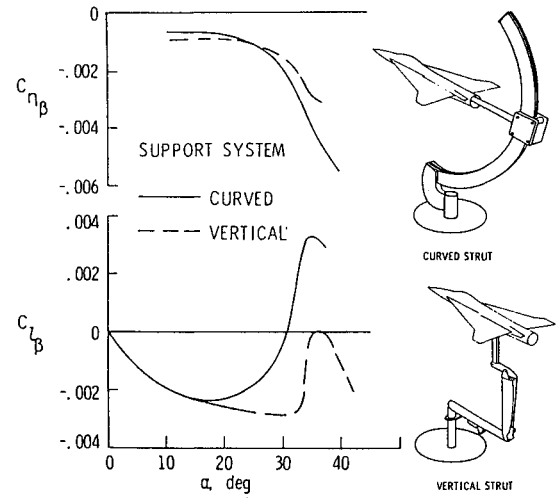

Fig. 11 Lateral-directional characteristics of an arrow wing at $\alpha = 35$ deg.[49]

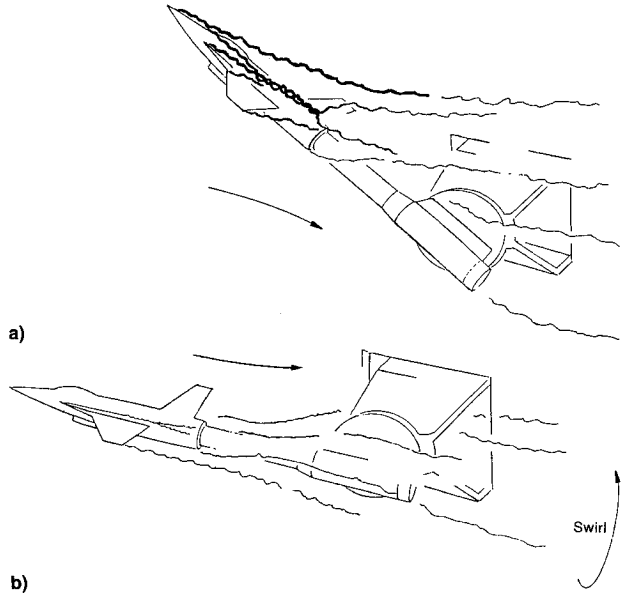

Fig. 12 Conceptual flowfield characteristics for sidewall support[9]: a) high and b) low α.

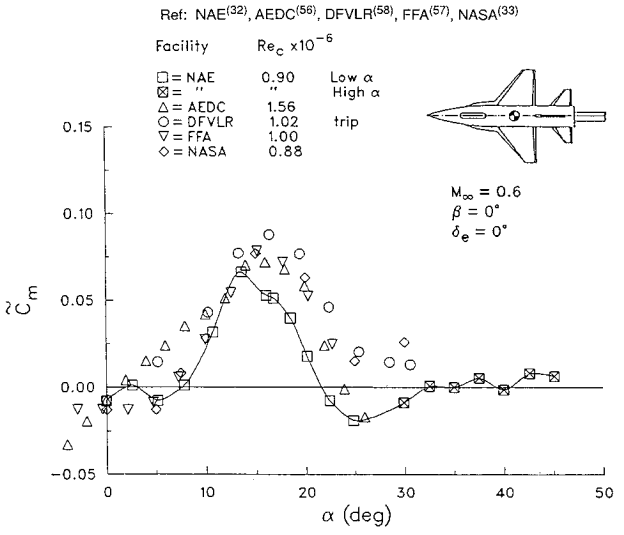

Fig. 13 SDM pitching moment characteristics.[48]

ever the type of support used, the associated self-excited support oscillation at high α can result in unwanted aerodynamic effects, in the worst case inhibiting the steady asymmetrical vortex shedding at high α.[55]

Planar Aerodynamic Characteristics

Oscillatory Pitching

The analysis of small-amplitude oscillatory experiments can elucidate the interactions between a model and support in related high-α experiments. For the example of the SDM at 35% mean aerodynamic chord, the pitching moment characteristics are relatively insensitive to Reynolds number at α up to 30 deg.[34] Therefore, the discrepancies[48] in C_m measured on sting-mounted models at $M_\infty = 0.6$ in several facilities[32,33,56-58] (Fig. 13) may be attributed, at least in part, to different levels of interference that could have been present in each of the tests, in particular near $\alpha = 0$ and at medium α. In contrast, support interference effects on pitch damping may be relatively benign on a configuration such as the SDM at $\alpha < 30$ deg.[59] In particular, sting interference effects on C^*_{mq} are small at $\alpha \leq 23$ deg.[60] Thus, the support interference has

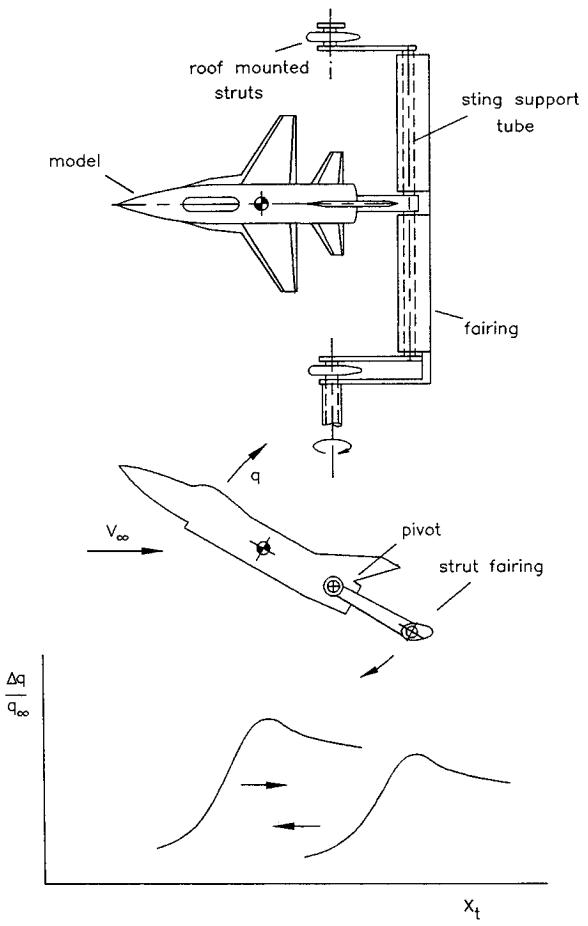

Fig. 14 Disturbances associated with pitching apparatus.

less effect on the time-lag-dominated pitch damping than on C_m.

Hybrid methods for wall corrections of dynamic derivatives at low α[61] may be applicable in this range. It is precisely in this domain, where the separated flows are reasonably well-behaved, that interference is not a problem; beyond this range massive separation occurs, followed by asymmetrical vortex shedding, and with it, facility interference effects rear their heads. The onset of this phenomenon will also be governed by pitch-rate-induced effects,[21] not present in the small-amplitude measurements.

Fixed-Axis Pitch-Up Experiments

All pitching apparatuses are subject to the salient facility interference mechanism at high α, namely, unsteady pressure gradients caused by variable wake blockage characteristics. For a model pitching within the poststall domain, the large effects of initial conditions,[62] pitch rate, and pivot point[21,62] can be studied by means of a cranked sting system, typified by the apparatus used at the Defence Research Agency in Bedford.[63]

If the model is to rotate about a fixed axis forward of the support, the strut will have to move relative to the test section reference. Conversely, if the strut is fixed, the model itself will traverse the test section, much as sketched in Fig. 2. For the geometry in Fig. 14, it follows that the disturbance caused by the horizontal strut supporting the sting will travel upstream with increasing α and, when the model is supported forward of the pivot axis, the disturbances due to the model and support will approach each other in the longitudinal direction as $\alpha \rightarrow 90$ deg. The latter geometry has the greatest potential for severe flowfield disturbances, which, being proportional to the wake blockage, vary in synchronism with the pitching cycle.

Wall static pressure signatures show that the disturbances caused by the model and strut at high α are felt across the entire test section.[9] An α increase is accompanied by an increase in wake blockage of the model together with upstream movement of the strut disturbance. Thus, the potential for test facility interference exists in pitching tests, increasing as the amplitude and/or frequency of the motion is increased, and is likely to be exacerbated at large offsets x_c, when the model motion relative to the test section reference is appreciable.

Unconstrained Planar Pitching

Figure 15 depicts a destabilized canard missile configuration in essentially planar flight in a wind tunnel[15] at $M_\infty = 0.7$. This case can more readily be related to actual flight conditions as support interference is absent, fluctuating blockage effects are minimal ($b/w \approx 0.06$), and viscous-flow/motion-coupling effects are negligible. Since the canard wake vortices actually impact on the tail fins at low-to-medium angles of attack, and the canard/wing separation is large, the aerodynamics are dominated by large convective time lag effects due to canard/wing interference (in Fig. 15 the canard wakes are moving away from the wing).

The directional damping derivative $C_{mq} + C_{m\dot{\alpha}}$ determined from near-planar flights (Fig. 3) using local aerodynamic analysis[65] (Fig. 16), reveals highly nonlinear behavior with complete loss of stability near $\alpha = 11$ deg.[66] Unlike oscillatory derivatives, the directional derivative embraces a limited time-history dependence.[29] Discrepancies between the sting-balance and free-flight aerodynamic characteristics[15] show that the aerodynamics are fundamentally different in the two cases. It has been recognized that under nonlinear conditions the entire motion history is relevant,[28,67] and, in this case, the missile flight provides the complete history of the nonoscillatory trajectory, with the true variations in rotation axis location (Fig. 3) and pitch rate. The key point here is that static and small-amplitude oscillatory experiments are not sufficient to predict the missile free-flight behavior, highlighting the needs for simulating the 6-DOF motion characteristics and for dealing with the associated dynamic support interference.

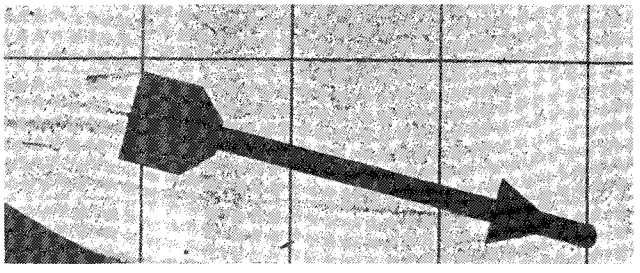

Fig. 15 Destabilized missile model in free flight.[66]

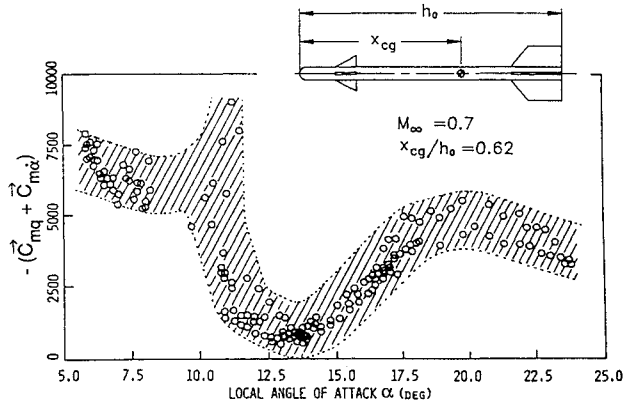

Fig. 16 Directional pitch-damping derivative in free flight.[66]

Nonplanar Aerodynamic Characteristics

Lateral-Directional Stability

For advanced aircraft configurations, the influence of a support strut can be particularly large in the α range dominated by forebody flow separation asymmetries. Figure 11 shows the different trends in $C_{n\beta}$ and $C_{l\beta}$ obtained with two different strut designs. Both systems cause significant interference,[42] but only the curved strut produces the strong-interaction interference on the asymmetrical forebody vortex pair (see Fig. 9). It is likely that similar differences in support interference contributed to the discrepancy between the $C_{n\beta}$ results obtained for the F-15 at 10 and 7.5% model scales in the Langley full-scale and Ames 12-ft wind tunnels[68] (Fig. 17).

On the other hand, considering the discrepancies between the wind-tunnel[68] and free-flight[69] data at the same Reynolds number, $Re = 4 \times 10^6$, it is evident that the maneuver input in the free-flight data had an effect at $\alpha \geq 35$ deg. The lower branch of the double-valued $C_{n\beta}$ was obtained from "maneuvers performed a few seconds before an unexplained rapid rolloff or upset."[69] A plausible, if inconclusive, explanation is that a finite yaw rate might have been present in those flights. Since the flow conditions on the translating forebody are supercritical at $Re = 4 \times 10^6$, the moving-wall effect would reinforce the flow separation asymmetry,[40] producing a propelling side force and, hence, a negative $C_{n\beta}$ increment. Thus, the viscous motion coupling and time-history effects have to be taken into account.

Lateral Support Oscillation

Since lateral oscillation of balance-mounted models will always be present at high α, the implications of motion coupling in "static" tests have to be considered. Results obtained for a secant-ogive-cylinder (SOC) demonstrated that the onset of asymmetrical vortex shedding is significantly delayed in the presence of yaw oscillation at an amplitude $\Delta\psi_z = \pm 1.5$ deg.[70]

Quantitative information has now been obtained at smaller amplitudes $\Delta\psi_z = \pm 0.4$ deg representative of high-α static tests on sting-mounted aircraft models.[64] The time-averaged static loads measured on the AGARD WG16A aircraft model under conditions of incipient vortex asymmetry were severely affected by yaw oscillation at this amplitude. The onset of asymmetry in $\bar{C}_n$ was delayed from $\alpha_{av} \approx 2\theta_a = 29$ deg to between 35–39 deg (Fig. 18). A nose-tip microasymmetry of $0.002d$ was sufficient to dominate over the oscillation-induced moving wall effect, resulting in asymmetry occurring near $\alpha_{av} \approx 29$ deg. This demonstrates that under these conditions static test data on models having slender symmetrical forebodies are not applicable to flight conditions. The applicable aerodynamic characteristics could be measured on a rotary apparatus,[55] provided that facility interference can be eliminated, as in the OPLEC apparatus.[9,27]

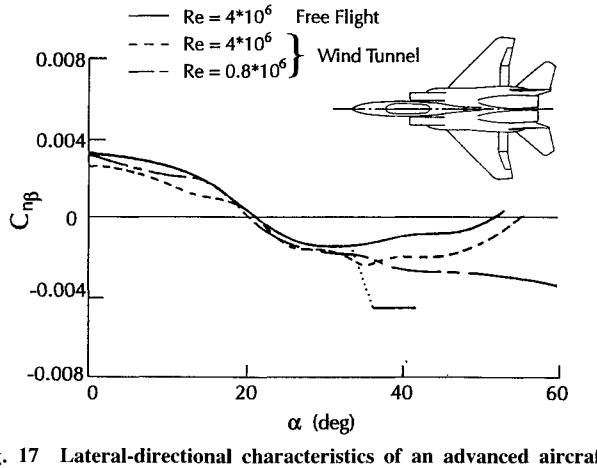

Fig. 17 Lateral-directional characteristics of an advanced aircraft model.[68,69]

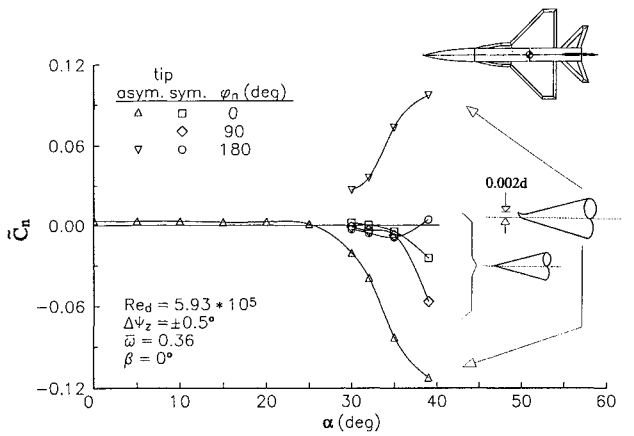

Fig. 18 Effects of yaw oscillation and nose tip microasymmetry on $\bar{C}_{n_\beta}$.[64]

Yaw- and Roll-Oscillation Experiments

Small test facility interference effects were detected[10] for a 65-deg delta wing in large-amplitude roll oscillation[20] with $b/w = 0.3$. For relatively large ratios b/w, significant unsteady wall interference may be present. The large undamping contributions of this interference present in yaw oscillation experiments of the SDM[32] ($b/w = 0.6$) prevented the determination of the yaw-oscillation characteristics at α above 28 deg. These effects were absent in subsequent experiments at $b/w = 0.32$.[64] To elucidate this phenomenon the SOC was oscillated[70] at different locations relative to the slotted wall $Y = (Y_0 - Y_T)/w$, where $Y_0 \approx w/2$ ($Y \approx 0.5$ on the tunnel centerline). Figure 19 demonstrates that the dynamic and static yaw derivatives are strongly influenced by wall interference at $\alpha \geq \alpha_{av}$. The undamping diminishes drastically as the wall is approached, demonstrating that C^*_{nr} cannot be determined at this level of unsteady wall interference.

Dynamic Cross-Coupling Derivatives

At low α and zero sideslip, the litmus test for accurate determination of cross-coupling pitching derivatives is the absence/presence of spurious cross-coupling contributions such as those evident in Fig. 20. The interfacility correlation[59] of $C^*_{l_q}$ data[32,56-58] on the SDM at $\beta = 0$ shows appreciable levels of measured dynamic cross-coupling at α below 19 deg. There is no physical basis for true aerodynamic cross coupling on the SDM at these conditions because the leading edge extension (LEX) vortex burst does not reach the trailing edge until $\alpha \approx 19$ deg,[32,64] which is also the attitude for symmetrical crossflow separation on the forebody ($\theta_a = 18.9$ deg). Thus, the measured effects must be attributed to combinations of measurement inaccuracies and unsteady interference effects peculiar to the individual test facilities.

As noted earlier, the strong-interaction type of interference is avoided at the expense of flowfield symmetry when an asymmetrical support strut is used, but significant test facility interference may yet be present at low α. To assess these effects in a small, slotted-wall test section, the SDM was set at $\alpha = 10$ deg and $\beta = \pm 5$ deg, and oscillated at an amplitude of ± 1 deg about the aerodynamic pitch axis.[9,48] When the angle between the symmetry planes of the model and the tunnel $\phi' = \hat{\phi} + n\pi$ was varied, the systematic effects were significant (Fig. 21). In the case of the rolling moment, the opposition between the interference contributions to the static and dynamic derivatives is characteristic of a convective flowfield time lag, and is, therefore, attributed to direct support interference.[48] In the absence of such a direct relationship, the systematic effects on the yawing moment derivatives (Fig. 21) must have been caused by a more complex flow mechanism, namely, unsteady, coupled support/wall interference.[9]

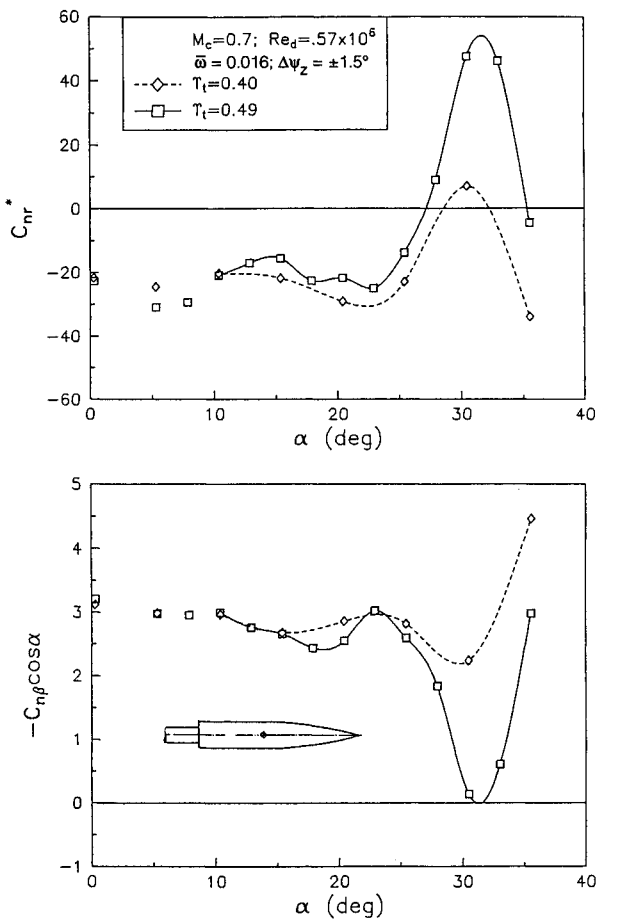

Fig. 19 Effect of slotted-wall proximity on the direct yawing-moment derivatives of a secant-ogive-cylinder.[70]

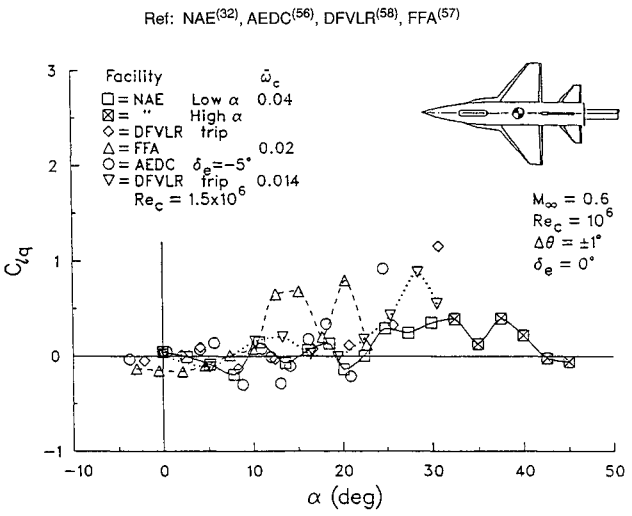

Fig. 20 Cross-coupling derivative due to pitch oscillation for SDM at $\beta = 0$ deg.[59]

At high α the strong interactions are eliminated since the vortex wake effectively passes above the support (Fig. 12). Instead, a form of coupled interference is present during pitch oscillation when disturbances originating at the slotted wall interact with the forebody/LEX vortex flows, both directly and by way of the support.[47] Evidence of unsteady wall interference[9] at high α was also found in the SDM roll[31]- and yaw-oscillation[32] results. From these findings and from the analysis of rotary data[9] it became apparent that, for models relatively large in relation to the test section size, $b/w \approx 0.6$,

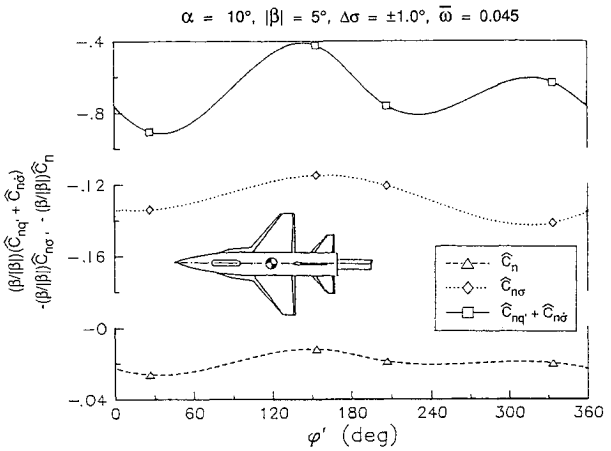

Fig. 21 Effect of model roll orientation on SDM yawing moment derivatives (M_∞ = 0.6).[9]

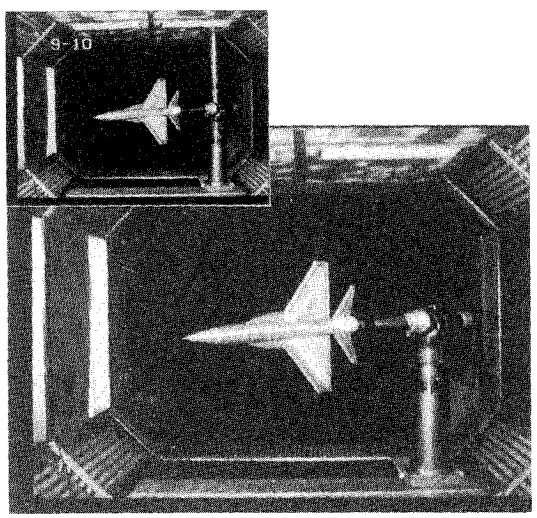

Fig. 22 AGARD WG16A model on asymmetrical support; with dummy strut (inset).[64]

the occurrence of test facility interference would be typical. Subsequent flowfield measurements[46] suggested the unsteady coupling effects become manageable at $b/w \leq 0.33$.[64]

With the AGARD WG16A model on the asymmetrical support in the IAR 2 × 3 m wind tunnel, depicted in Fig. 22, b/w = 0.36, and the weak-interaction facility interference was relatively benign.[64] In contrast to the data in Fig. 20 the aerodynamic cross coupling is effectively nonexistent below α = 30 deg, as expected (Fig. 23). Significant levels of cross coupling develop in the region of steady asymmetrical vortex shedding (30 deg $\leq \alpha \leq$ 45 deg). To investigate the effects of support asymmetry, a nonstructural dummy strut was installed, completing the mirror image of the support in the horizontal pitch plane[46] (Fig. 22). The effects of the support asymmetry are significant,[64] and also complex because they are strongly coupled with the motion-induced effects, particularly in the region of incipient asymmetrical vortex shedding, 25 deg $\leq \alpha \leq$ 32 deg (Figs. 23 and 24). Figure 24 illustrates how the onset of unsteady side force asymmetry is promoted by the strut asymmetry to occur at $\alpha_{av} \approx$ 30 deg, compared to $\alpha_{av} \approx$ 32 deg with the dummy.

Large differences in C^*_{nq} were measured on the SDM with and without the dummy strut at β = 0, in the range 42 deg $\leq \alpha \leq$ 53 deg.[64] It is thought that in this range, where the symmetrizing influence of the LEXs is rapidly diminishing, the coupling between the forebody and LEX vortices is particularly sensitive to the motion-induced fluctuations covected from the flowfield near the strut, resulting in large disturbances in the region near the tail fin. This interpretation is consistent with buffet measurements on the same model[71]; at α = 42 deg and $\beta \neq$ 0, the buffet excitation on the fin was not symmetrical with respect to β = 0, suggesting the presence of a lateral bias in the concentrations of vorticity near the fin.

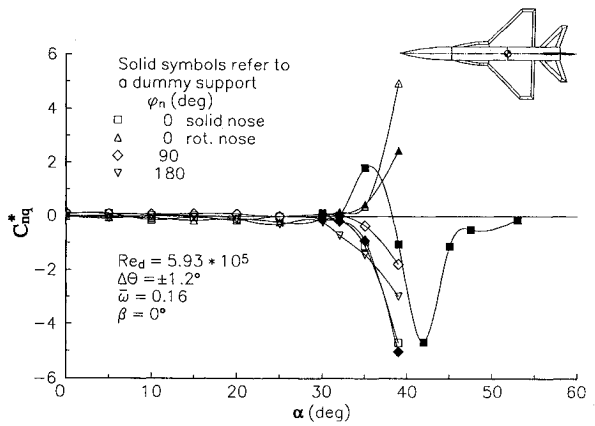

Fig. 23 Cross-coupling derivative due to pitch oscillation for AGARD WG16A model.[64]

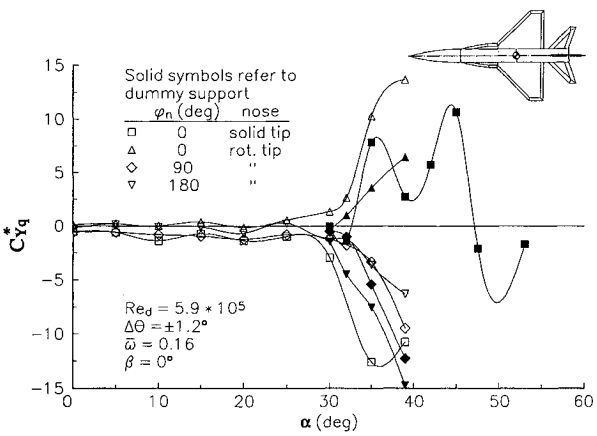

Fig. 24 Dynamic side-force derivative in pitch oscillation for AGARD WG16A model.[64]

Use of the dummy strut does not eliminate the interference, but replaces the asymmetrical type of facility interference with a symmetrical flow disturbance similar to that associated with the pitch/heave rig concept[63] (see Fig. 14). Since the symmetrical disturbance will minimize the effect on the forebody flow asymmetry, this support will make it possible to determine the cross-coupling derivatives. On the other hand, the increased wake blockage caused by the dummy strut will result in stronger fluctuating upstream pressure gradients with a concomitantly larger effect on the in-plane derivatives.[64] Thus, at high α the determination of direct and cross-coupling derivatives can lead to conflicting requirements, indicating a need for tests both with and without the dummy strut.

Effects of Sideslip

Below $\alpha = \alpha_{av}$ the determination of C^*_{nq} and C^*_{lq} is less problematic at finite β, where there is a set flow asymmetry. Nevertheless, the support will produce some asymmetry because the downwash directions are different functions of the pitch angle at positive and negative β.[46] For brevity, results at $\beta \neq 0$[3,32,64] are not included, but the conclusion is the same; the cross-coupling derivative data may not be useful if the effects of experimental constraints are not accounted for. A ventral blade support[72] is useful when the model base geometry should not be modified, but introduces a form of dynamic support interference that is exacerbated by the presence of finite sideslip angles.

Nonlinear Aerodynamics

The above analysis is based on, but not restricted to, aerodynamic characteristics expressed in terms of locally linear derivatives. The results in Figs. 23 and 24 show that stability derivatives are not directly useful in simulations of poststall maneuvers, but provide insight into the unsteady facility interference mechanisms associated with a pitching or yawing model. The analysis of nonlinear aerodynamic measurements would present particular difficulties because the interference contributions to measured unsteady airloads or pressures are indistinguishable from the vehicle aerodynamics, and will, therefore, be reduced as spurious nonlinear effects. Thus, locally linear data obtained for prescribed characteristic motions are likely to remain an important diagnostic tool. That the interference phenomena are themselves dependent on the motion characteristics is amply demonstrated by the foregoing results. This underscores the need for adequate 6-DOF motion simulation. When time history effects are important, and/or support interference has to be eliminated, validation through free-flight techniques[15,69,73] is indicated.

Rotary Aerodynamic Characteristics

The unsteady aerodynamic interference phenomena germane to high-α oscillatory experiments have their counterparts in rotary balance tests, although the mechanisms that produce them are quite different here. The ubiquitous support interference in rotary experiments[42,74] derives from the presence of a rotating support arm, which produces a strong-interaction type of interference by obstructing the vortical flows shed from models of advanced aircraft. In the interests of rigidity, the rotary balance support is typically quite bulky (Fig. 25), but it is its proximity to the model, rather than its size, that produces this type of interference. On the other hand, the wake blockage produces upstream pressure gradients that can lead to facility interference effects.[47] When $b_s/w < 0.4$, unsteady separation on the walls should not occur,[9] then the blockage-induced dynamic pressure rise is stationary in the longitudinal sense, and could, therefore, be alleviated by adaptive wall technology.[61]

Support Interference

The interference is basically steady in lunar coning motion (Fig. 6 with $\lambda = 0$). Because of the coning-induced tilting of the forebody vortices, the active vortex could miss the rotor arm at certain α-β combinations when Ω is high enough,[74] thereby alleviating the interference. However, some residual interference may still be present owing to the distortion of the flowfield by the rotor arm.

In rotary tests of a model of an advanced aircraft, both aft- and top-mounted sting systems were used at $\alpha = 70$ deg[75] (Fig. 26). For the configuration with nose boom and sting angle $\alpha_s = 70$ deg, critical flow separation conditions appear to be present on the forebody.[74] Thus, the coupling between the moving-wall effects and the strong-interaction interference of the dorsal sting causes the vortex asymmetry to flip between the two extreme positions, with resulting reversals and hysteresis in the $C_n - \bar{\Omega}$ characteristics.

The strong-interaction is a function of α, β, $\bar{\Omega}$, and support geometry. At certain attitudes the differences between effects of two alternative mounting systems may disappear; however, this does not mean that the support interference has disappeared, but rather that the associated strong interaction has become ineffective. For instance, in tests of an aft-mounted HIRM 2 model,[76,77] a dummy sting[76] contributed significantly to the support interference on C_l at $\alpha = 40$ deg, and C_n at $\alpha = 60$ deg (Fig. 27), but at $\alpha = 50$ deg the vortex burst was apparently moved up far enough upstream that there was no appreciable effect. It is likely that at $\alpha = 40$ deg the effects on C_l were caused by the interaction of the inboard forebody vortex with the canard vortices, which would be strongly affected by the dummy strut. At high α, the aerodynamic characteristics are dominated by the asymmetric forebody vortex pair, which is unaffected by the canard at $\alpha = 60$ deg, resulting in asymmetrical side forces on the forebody in coning motion.

Test Facility Interference

In a rotary test, vortices generated by the forebody and lift surfaces are convected downstream as coaxial helical structures of common pitch. The close proximity of wind-tunnel boundaries could distort these vortex formations cyclically. This has been referred to as vortex-wake/wall interference.[9,47] When the span of the rotor arm is large, $b_s > b$, the trailing tip vortices will be the prime source of vortex-wake/wall interference. As the vortex trails move towards or away from a point on the wall, boundary-layer separation could occur on the wall or further downstream, in the diffuser (Fig. 28). Thus, the separation line on the wall/diffuser would oscillate longitudinally while traveling in the direction of the rotation, with concomitant wake blockage fluctuations.

Tests were conducted with the HIRM 2 model on the same apparatus in a 4 × 2.7 m low-speed wind tunnel (LSWT), and in a 2.4 × 1.8 m variable-density transonic wind tunnel (TWT)[76] (Fig. 25). The relative dimensions were $b_s/w = 0.4$ and 0.6, respectively. A comparison revealed dramatic discrepancies between the C_n characteristics measured in the two

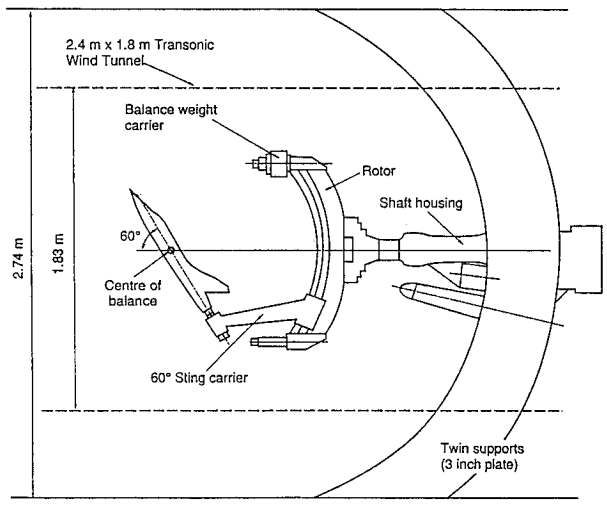

Fig. 25 Layout of RAE rotary balance in 4 × 2.7 m low-speed wind tunnel.[76]

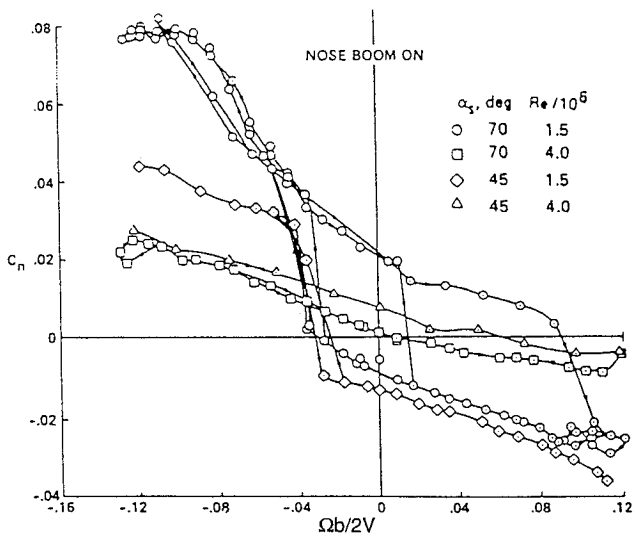

Fig. 26 $C_n(\bar{\Omega})$ characteristics of advanced aircraft model at $\alpha = 70$ deg, $\beta = 0$ deg.[75]

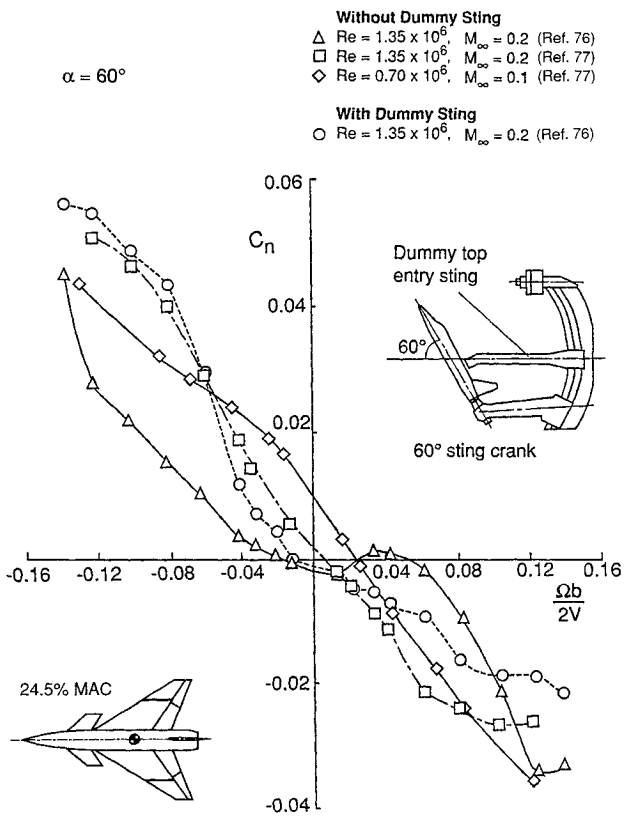

Fig. 27 Yawing moment data for HIRM 2 in 4 × 2.7 m low-speed wind tunnel.[76,77]

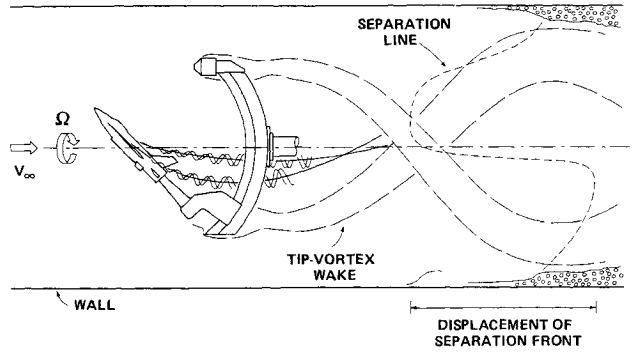

Fig. 28 Coupled support/wall interference in rotary test.[9]

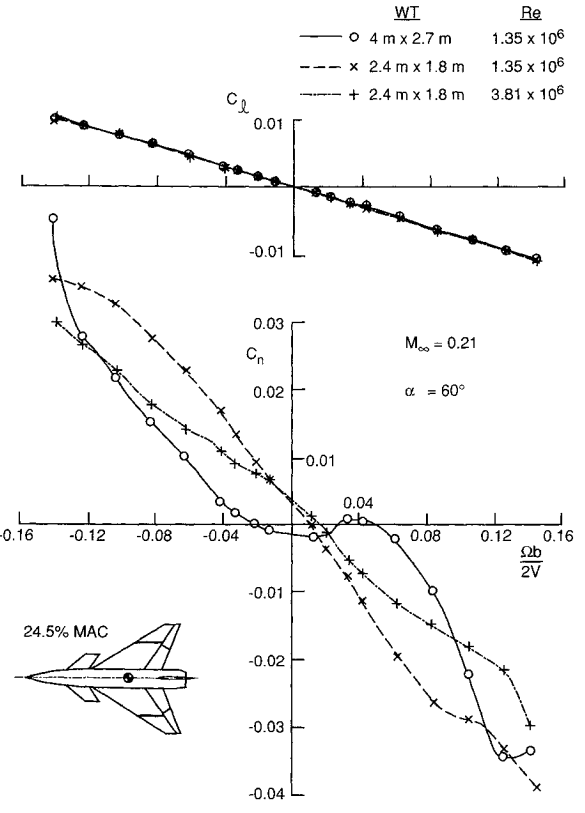

Fig. 29 Comparison of HIRM 2 results from two wind tunnels (LE droop of 12.5 deg).[76]

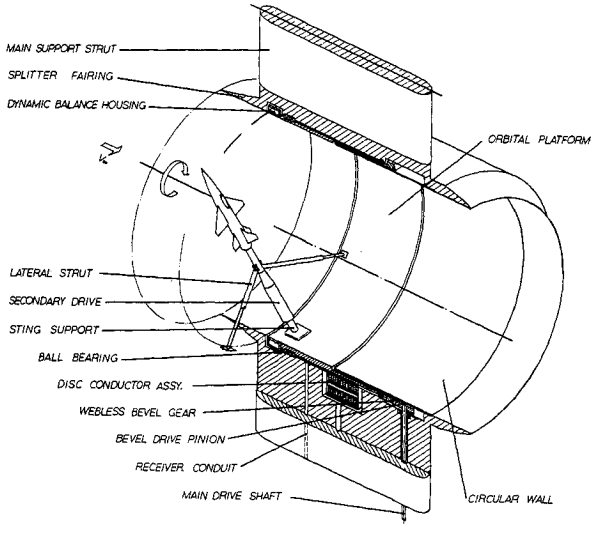

Fig. 30 Layout of the OPLEC apparatus.[27]

facilities at the same Reynolds number (Fig. 29). Moreover, the observations in the large test section[76,77] demonstrate a variety of types of nonlinear behavior (Fig. 27). In contrast, in the smaller facility the characteristics are nearly linear over the complete $\Omega b/2V$ range at both Reynolds numbers,[9] with no hint of the *Re*-critical behavior expected at $Re = 1.35 \times 10^6$.

These phenomena were analyzed in detail.[9] In essence, the interpretation given suggests that the forebody/canard leading-edge vortices are drawn laterally into the low-pressure regions between the rotor arm, hub, and the walls (Fig. 28), and will, therefore, be periodically deflected laterally. The oscillatory constraint on the pressure gradients downstream of the model will inhibit the flow separation dynamics. The flow separation on the forebody appears to alternate between the subcritical and critical type with accompanying reversals in the moving wall effect.[9] Because of the forebody shape transition[76] of HIRM 2, the subcritical/critical interaction region is small so that the effects on C_n are gradual in the LSWT (Figs. 27 and 29), rather than abrupt as in Fig. 26. As with the oscillatory results discussed earlier,[70] the oscillation-induced moving wall effect prevents the subcritical flow separation asymmetry from being established; thus, the oscillatory input results in a zero time-averaged effect on C_n.[9] Since these effects tend to increase with increasing rotation rate, the yawing moment would also increase with coning rate, resulting in a roughly linear $C_n - \Omega b/2V$ trend in the TWT (Fig. 29). The unsteady facility interference is apparently negligible in the larger tunnel, allowing the existence of steady support interference.

From these results, it is clear that quite erroneous interpretations of the vehicle rotary aerodynamic characteristics could be made if the nature of the test facility interference/motion-coupling effects are not understood. For instance, in the case of HIRM 2, it would not be known whether the yawing moment characteristics in a steady spin will be stable

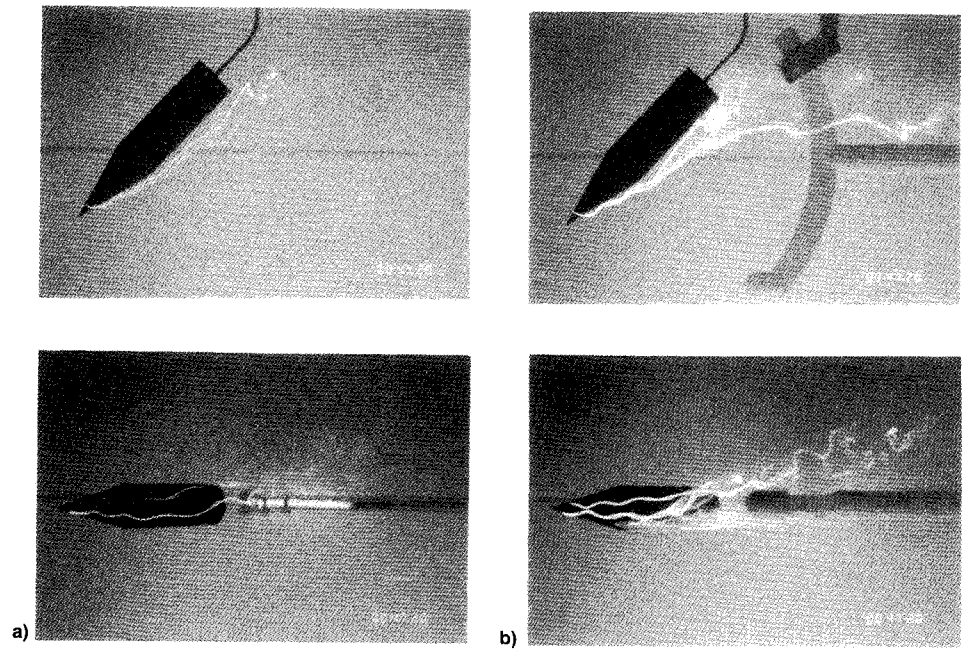

Fig. 31 Flow visualization 15-deg cone-cylinder coning at α = 47 deg and $\hat{\Omega}$ = 0.2[78]: a) without dummy rotor and b) with dummy rotor.

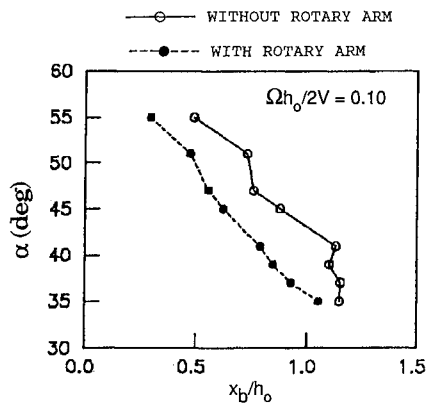

Fig. 32 Effect of dummy rotor arm on longitudinal location of breakdown of inboard vortex.[78]

or unstable at α = 60 deg, unless the experimental data are correctly interpreted.

Alleviation of Support Interference

It has been pointed out that the individual contributions of various sources of interference cannot be separated on a conventional rotary balance, and that a more sophisticated approach is required.[47] A rotary-balance technique offering the necessary flexibility was recently proposed.[9,47] The so-called orbital-platform, or OPLEC, apparatus[27] (Fig. 30) makes it possible, in principle, to simulate separately (or in combination) the effects of the walls and of the rotating arm[78] and fixed struts. Application of the OPLEC concept could eliminate most of the problems identified here in connection with rotary balance testing; strong-interaction support interference is eliminated by virtue of the absence of the centrally mounted support arm found in conventional rotary apparatuses, and unsteady wall interference is negligible with the circular test section geometry (Fig. 30).

In a recent water-tunnel experiment,[78] a 15-deg half-angle cone-cylinder was tested on an OPLEC apparatus. The model was mounted on a sting attached to an external annular platform riding on the outer surface of a cylindrical test section insert.[27] A dummy rotating arm was attached to the sting/strut to simulate the support interference effects in conventional rotary tests. Flow visualization revealed significant differences in the flowfields generated with and without the dummy rotor arm over an α range bracketing the region of steady asymmetrical vortex shedding (Fig. 31). Not only was vortex breakdown significantly promoted by the presence of the dummy arm (Fig. 32), but topological changes in the flowfield were encountered at several α, Ω combinations[78] (Fig. 31). Bifurcation of the inboard vortex could be triggered by the presence of the dummy arm at certain combinations of α and Ω, whereas at others significant reverse flows were established (Fig. 31b), that were not present in the absence of the arm. This experiment serves to substantiate the previous analyses of strong-interaction interference,[9,42,74] and illustrates how erroneous interpretations of vehicle dynamics can result when such effects prevail.

Arbitrary Nonplanar Maneuvers

The measure of success achieved in maneuver predictions depends on the capability for utilizing dynamic data from diverse sources, including oscillatory, rotary, and free-flight experiments. Since high-α aerodynamic characteristics can be highly sensitive to experimental conditions, it is imperative that the correct interpretation be obtained in each case. When direct application of experimental data is ruled out, numerical/analytical techniques must be used to extend their applicability. In practice, this means that dynamic experiments (which might involve motion constraints or deficient Reynolds numbers), be used to validate CFD or macro-aerodynamics models for extrapolation to flight conditions.

Experimental Methods

Data Correlation

From comparisons of dynamic data[79] on HIRM 1 and on HIRM 2 it is obvious that the correlation of rotary and oscillatory (and free-flight) data is not straightforward. The systematic correlation[30] of SDM oscillatory and rotary data based on one mathematical model, Eq. (3), illustrates how interference effects on the dynamic derivatives can complicate the application to flight prediction. Unsteady wall interference effects in the oscillatory derivatives [Eq. (2)], and weak-interaction support interference in the coning derivative are likely to have contributed to the discrepancy between the two terms in Fig. 7. Thus, the application of mathematical models

based on the synthesis of the responses to individual rotary and oscillatory motions may be inconclusive or even meaningless unless the facility interference contributions have been identified.

Multi-DOF Captive Model Experiments

Predictive flight dynamic analysis of specific aircraft behavior in the poststall domain would require more complex 2-DOF experiments. Of the techniques for producing complex motions, oscillatory coning[80] is the simplest. In the so-called "tournebroche," the coning axis is inclined ($\lambda \neq 0$ in Fig. 6). The single-DOF motion generates high rates of change of α and β at large values of λ. Unsteady support interference and, possibly, facility interference is unavoidable because of the oscillatory flow conditions. It will not be possible to uncouple the unsteady interference from the vehicle aerodynamics when strong viscous flow/motion coupling is present, but the interference can be analyzed by considering the effects of λ and Ω. To a lesser degree this is also true of the epicyclic orbital-platform concept[27] (OPLEC), which could be used to generate arbitrary 2-DOF epicyclic motion at high α. Although the strong-interaction and vibration-induced interference is largely absent in this case, unsteady wall interference may result for large values of b/w. In short, there is a potential for unsteady interference whenever the forced motion is asymmetrical.

6-DOF Flight Predictions

Simulation of aircraft oscillatory spinning requires a mathematical model such as the nonlinear counterpart of Eq. (1), in which the nonlinear motion-rate dependence is incorporated in the functional formulation.[28] Since the reactions are again synthesized from the unsteady reactions to individual characteristic motions,[27,28] the predictions can only be reliable if all of the inputs to the mathematical model are free of significant interference. Where the inputs are compromised by strong motion/interference coupling, the correct interpretation may have to be obtained from hybrid free-flight/analytical methods.

Free-Flight Techniques

Wind-tunnel free-flight experiments[15,66] are restricted to low Reynolds numbers, but arbitrary angles of attack and sideslip and very high angular rates can be attained. Such tests could be sensitive to test-section flow nonuniformity.[22] However, the main challenge is to achieve sufficient control over initial conditions that appropriate nonplanar trajectories can be generated. An example may be found in the planar free-flight study[15,66] (Fig. 15). The reactions are highly nonlinear, and finite, if small, roll rates are unavoidable as a result of aerodynamic cross coupling. Thus, the separated flowfields are chaotic, and an infinite variety of nonplanar trajectories could result from the same set of initial conditions. To obviate this behavior fin roll tabs were used to generate a rolling moment, and the model was prespun in the opposite direction at launch[66] to achieve zero roll rate at the peak angle of attack. When high Reynolds numbers are required, alternative techniques such as the free-flight catapult facility[73] and model-scale flight tests[69,79] can be used.

Hybrid Experimental/Numerical Simulations

For the purposes of code validation, free-flight techniques are suitable because they eliminate the complication of test facility interference. Moreover, to develop CFD simulations, the free-flight motion history can be used as input to a forced-motion numerical simulation and the computed evolution of the flowfield compared with its free-flight counterpart. A consequence of the presence of facility interference and kinematic constraints, limiting the applicability of dynamic data, is an increase in complexity of the flight dynamic model (Fig. 1). In maneuvering flight changes in flow state are dependent upon the time history of the motion variables, which is correctly simulated in free-flight experiments (Fig. 16). Using the insight into the nonlinear flight dynamic phenomena gleaned from these flights, the global 6-DOF model can be constructed in such a way as to systematically employ the data from experimental and computational sources.

Conclusions

The principal conclusions of this Paper may be summarized as follows.

1) Interpretations of high-α data should be founded on analyses of the flow physics involved as spurious contributions to measured characteristics and can lead to unrealistic flight predictions.

2) The aerodynamics of advanced aircraft can be strongly maneuver-coupled at high α; therefore, the different kinematic and time-history dependent inputs to the wind-tunnel data and in flight, have to be taken into account.

3) The interpretation given to high-α dynamic data can be a key factor in determining the structure of the nonlinear aerodynamic mathematical model.

4) Ground test facility interference can be inextricably coupled with viscous motion-induced flow effects and becomes particularly significant when asymmetrical vortex shedding occurs.

5) Although not directly useful in poststall maneuver simulation, oscillatory derivatives provide an important diagnostic tool for interpretation of unsteady interference effects.

6) Free-flight experiments can provide the physical analogue of flight required for data interpretation and code validation.

References

[1]Rom, J., *High Angle of Attack Aerodynamics*, 1st ed., Springer–Verlag, New York, 1992.

[2]Altenkirch, D., "Flugmech. Anal. der dyn. Derivative des Dornier-Variations-modells," DFVLR-FB-83-38, Brunswick, Germany, Nov. 1993.

[3]Edwards, J. W., "Assessment of Computational Prediction of Tail Buffeting," NASA-TM-101613, Jan. 1990.

[4]Kutler, P., and Gross, A. R., "Progress and Future Directions in Computational Fluid Dynamics," NASA-TM-100091, June 1988.

[5]Hoeijmakers, H. W. M., "Modeling and Numerical Simulation of Vortex Flow in Aerodynamics," *Vortex Flow Aerodynamics*, Paper 1, AGARD-CP-494, July 1991.

[6]Bobbitt, P. J., "The Pros and Cons of Code Validation," NASA-TM-100657, July 1988.

[7]Ericsson, L. E., and Reding, J. P., "Review of Support Interference in Dynamic Tests," *AIAA Journal*, Vol. 21, No. 12, 1983, pp. 1652–1666.

[8]Acum, W. E. A., "Interference Effects in Unsteady Experiments," AGARDograph 109, Oct. 1966, pp. 219–278, Chap. 4.

[9]Beyers, M. E., "Unsteady Wind-Tunnel Interference in Aircraft Dynamic Experiments," *Journal of Aircraft*, Vol. 29, No. 6, 1992, pp. 1122–1129.

[10]Beyers, M. E., and Ericsson, L. E., "Ground Facility Interference on Aircraft Configurations with Separated Flow," *Journal of Aircraft*, Vol. 30, No. 5, 1993, pp. 682–688.

[11]Polhamus, E. C., "A Review of Some Reynolds Number Effects Related to Bodies at High Angles of Attack," NASA-CR-3809, Aug. 1984.

[12]Helin, H. E., Schreck, S. J., Bohney, D. V., and Durant, V. M., "Effects of Freestream Turbulence on Dynamic Stall," *Journal of Aircraft* (submitted for publication).

[13]Ericsson, L. E., "Effects of Transition on Wind Tunnel Simulation of Vehicle Dynamics," *Progress in Aerospace Sciences*, Vol. 27, No. 2, 1990, pp. 121–144.

[14]Ericsson, L. E., and Beyers, M. E., "Viscous-Flow/Vehicle-Motion Coupling," AGARD-AR-265, Dec. 1990, pp. 164–187, Chap. 8.3.

[15]Beyers, M. E., "Free-Flight Investigation of High-Maneuverability Missile Dynamics," *Journal of Spacecraft and Rockets*, Vol. 14, No. 4, 1977, pp. 224–230.

[16]Ericsson, L. E., "Moving Wall Effect in Relation to Other Dynamic Stall Mechanisms," *Journal of Aircraft*, Vol. 31, No. 6, 1994, pp. 1303–1309.

[17]Bihrle, W., Tristrant, D., Valtorta, E., O'Leary, C. O., Beyers, M. E., and Malcolm, G. N., "Use of Rotary-Balance Data in the Prediction of Aircraft Dynamics," AGARD AR-265, Dec. 1990, pp. 188–208, Chap. 9.

[18]Tobak, M., and Chapman, G. T., "Nonlinear Problems in Flight Dynamics Involving Aerodynamic Bifurcations," AGARD-CP-386, Paper 25, Nov. 1985.

[19]Gad-el-Hak, M., and Ho, C.-M., "The Pitching Delta Wing," *AIAA Journal*, Vol. 23, No. 9, 1990, pp. 1660–1665.

[20]Hanff, E. S., and Jenkins, S. B., "Large-Amplitude High-Rate Rolling Experiments on a Delta and Double Delta Wing," AIAA Paper 90-0224, Jan. 1990.

[21]Helin, H. E., and Walker, J. M., "Interrelated Effects of Pitch Rate and Pivot Point on Airfoil Dynamic Stall," AIAA Paper 85-0130, Jan. 1985.

[22]Beyers, M. E., "The Problem of Wind Tunnel Flow Nonuniformity in Free-Model, Aircraft Dynamic Stability Tests," Council for Scientific and Industrial Research, NIAST Rept. 79/39, Pretoria, South Africa, April 1979.

[23]Herbst, W. B., "Future Fighter Technologies," *Journal of Aircraft*, Vol. 17, No. 8, 1980, pp. 561–566.

[24]Tristrant, D., "ONERA-IMFL—Correlation with Flight Tests," AGARD-AR-265, Dec. 1990, pp. 217–229, Chap. 11.3.

[25]Bihrle, W., Jr., and Barnhart, B., "Spin Prediction Techniques," *Journal of Aircraft*, Vol. 20, No. 2, 1983, pp. 97–101.

[26]Orlik-Rückemann, K. J., "Dynamic Stability Testing in Wind Tunnels," National Research Council, NAE-LTR-UA-41, Ottawa, Canada, March 1977.

[27]Beyers, M. E., and Huang, X. Z., "The Orbital Platform Concept for Nonplanar Dynamic Testing," National Research Council, NAE-AN-52, Ottawa, Canada, May 1988.

[28]Tobak, M., and Schiff, L. B., "On the Formulation of the Aerodynamic Characteristics in Aircraft Dynamics," NASA TR R-456, Jan. 1976.

[29]Beyers, M. E., "A New Look at the Tobak-Schiff Model of Nonplanar Aircraft Dynamics," National Research Council, NAE-LTR-UA-101, Ottawa, Canada, Dec. 1989.

[30]Beyers, M. E., "Correlations Based on Mathematical Model," AGARD-AR-265, Dec. 1990, pp. 210–214, Chap. 10.2.

[31]Beyers, M. E., "Subsonic Roll Oscillation Experiments on the Standard Dynamics Model," AIAA Paper 83-2134, Aug. 1983.

[32]Beyers, M. E., "SDM Pitch- and Yaw-Axis Stability Derivatives," AIAA Paper 85-1827, Aug. 1985.

[33]Jermey, C., and Schiff, L. B., "Wind-Tunnel Investigation of the Aerodynamic Characteristics of the Standard Dynamics Model in Coning Motion at Mach 0.6," AIAA Paper 85-1828, Aug. 1985.

[34]Huang, X. Z., and Beyers, M. E., "Subsonic Aerodynamic Coefficients of the SDM at Angles of Attack up to 90°," National Research Council, NAE-LTR-UA-93, Ottawa, Canada, Jan. 1980.

[35]Orlik-Rückemann, K. J., "Sensitivity of Aircraft Motion to Cross-Coupling and Acceleration Derivatives," AGARD-LS-114, Paper 15, May 1981.

[36]Chaderjian, N., and Schiff, L. B., "Navier-Stokes Prediction of a Delta Wing in Roll with Vortex Breakdown," AIAA Paper 93-3495, Aug. 1993.

[37]Mendenhall, M. R., Perkins, S. C., Jr., and Lesieutre, D. J., "Vortex Cloud Model for Body Vortex Shedding and Tracking," *Tactical Missile Aerodynamics: Prediction Methodology*, edited by A. R. Seebass, Vol. 142, Progress in Astronautics and Aeronautics Series, AIAA, Washington, DC, 1992, pp. 225–285.

[38]Huang, X. Z., and Hanff, E. S., "Prediction of Normal Force on a Delta Wing Rolling at High Incidence," AIAA Paper 93-3686, Aug. 1993.

[39]Gallaway, C. R., and Hankey, W. L., "Free-Falling Autorotating Plate—A Coupled Fluid and Flight Mechanics Problem," *Journal of Aircraft*, Vol. 22, No. 11, 1985, pp. 983–987.

[40]Ericsson, L. E., "Moving Wall Effects in Unsteady Flow," *Journal of Aircraft*, Vol. 25, No. 11, 1988, pp. 977–990.

[41]Ericsson, L. E., "The Moving Wall Effect vis-à-vis Other Dynamic Stall Flow Mechanisms," AIAA Paper 93-3424, Aug. 1993.

[42]Ericsson, L. E., and Reding, J. P., "Dynamic Support Interference in High-Alpha Testing," *Journal of Aircraft*, Vol. 23, No. 12, 1986, pp. 889–896.

[43]Hummel, D., "Untersuchungen über das Aufplatzen der Wirbel an schlanken Delta Flügeln," *Z. für Flugwissenschaften*, Vol. 3, Heft. 5, 1965, pp. 158–168.

[44]Ericsson, L. E., and Reding, J. P., "Asymmetric Vortex Shedding from Bodies of Revolution," *Tactical Missile Aerodynamics*, Vol. 104, AIAA, Progress in Astronautics and Aeronautics, Washington, DC, 1986, pp. 243–296.

[45]Reding, J. P., and Ericsson, L. E., "Dynamic Support Interference," *Journal of Spacecraft and Rockets*, Vol. 9, No. 7, 1972, pp. 547–553.

[46]Beyers, M. E., Cai, H. J., and Penna, P. J., "Flow-Field Interference Produced by an Asymmetrical Support Strut," National Research Council, Inst. for Aerospace Research, IAR-AN-75, Ottawa, Canada, Jan. 1993.

[47]Beyers, M. E., "Unsteady Wall Interference in Rotary Tests," AIAA Paper 89-0046, Jan. 1989.

[48]Beyers, M. E., "Some Recent NAE Experiences of Support Interference in Dynamic Tests," National Research Council, NAE-LTR-UA-83, Ottawa, Canada, Nov. 1985.

[49]Johnson, J. L., Jr., Grafton, S. B., and Yip, L. P., "Exploratory Investigation of the Effects of Vortex Bursting on the High Angle-of-Attack Lateral-Directional Stability Characteristics of Highly-Swept Wings," AIAA Paper 80-0463, March 1980.

[50]Ericsson, L. E., "Effect of Sting Plunging on Measured Nonlinear Pitch Damping," AIAA 78-832, April 1978.

[51]Burt, G. E., and Uselton, J. C., "Effect of Sting Oscillations on the Measurement of Dynamic Stability Derivatives," *Journal of Aircraft*, Vol. 13, No. 3, 1976, pp. 210–216.

[52]Canu, M., "Mesure en soufflerie de l'amortissement aérodynamique en tangage d'une maquette d'avion oscillant suivant deux degrés de liberté," *La Recherche Aérospatiale*, No. 1971-5, Sept.–Oct. 1971, pp. 257–267.

[53]Beyers, M. E., "Direct Derivative Measurements in the Presence of Sting Plunging," *Journal of Aircraft*, Vol. 23, No. 3, 1986, pp. 179–185.

[54]Beyers, M. E., "Influence of Support Oscillation in Dynamic Stability Tests," *Journal of Aircraft*, Vol. 25, No. 2, 1988, pp. 178–183.

[55]Ericsson, L. E., "Lateral Oscillations of Sting-Mounted Models at High Alpha," *Journal of Spacecraft and Rockets*, Vol. 27, No. 5, 1990, pp. 508–513.

[56]Coulter, S. M., and Marquart, E. J., "Cross and Cross-Coupling Derivative Measurements on the Standard Dynamics Model at AEDC," AIAA Paper 82-0596, March 1982.

[57]Torngren, L., "Dynamic Pitch and Yaw Derivatives of the Standard Dynamics Model," FFA TN 1985-5, Stockholm, Sweden, 1985.

[58]Schmidt, E., "Standard Dynamics Model Experiments with the DFVLR/AVA Transonic Derivative Balance," AGARD CP-386, May 1985.

[59]Beyers, M. E., "Interfacility Correlation and Analysis of SDM Derivatives at Mach 0.6," National Research Council, Ottawa, Canada (to be published).

[60]Cyran, F. B., "Sting Interference Effects on the Static, Dynamic, and Base Pressure Measurements of the Standard Dynamics Model Aircraft at Mach Numbers 0.3 Through 1.3," Arnold Engineering Development Center, AEDC-TR-81-3, Aug. 1981.

[61]Kuczka, D., "Hybridverfahren für instantionäre Messungen in transsonischen Windkanälen am Beispiel der harmonischen Nickschwingung," DFVLR-Forschungsbericht 88-19, Göttingen, Germany, 1988.

[62]Jarrah, M.-A. M., "Low-Speed Wind-Tunnel Investigation of Flow About Delta Wings, Oscillating in Pitch to Very High Angle of Attack," AIAA Paper 89-0295, Jan. 1989.

[63]O'Leary, C. O., and Rowthorn, E. N., "Low Speed Dynamic Tests on a Canard Configured High Incidence Research Model (HIRM 2)," RAE-TR-88024, Farnborough, Hants, England, UK, Dec. 1987.

[64]Cai, H. J., Beyers, M. E., and Elias, S., "Oscillatory Experiments on the AGARD WG16A Model," National Research Council, Ottawa, Canada (to be published).

[65]Beyers, M. E., "Technique for Smoothing Free-Flight Oscillation Data," *Journal of Spacecraft and Rockets*, Vol. 12, No. 5, 1975, pp. 318, 319.

[66]Beyers, M. E., "Investigation of High-Maneuverability Flight Vehicle Dynamics," International Council of the Aeronautical Sciences, ICAS-80-7.2, Oct. 1980.

[67]Cunningham, A. M., and den Boer, R. G., "Analysis of Unsteady Force, Pressure and Flow-Visualization Data for a Pitching Straked Wing Model at High Angles of Attack," AGARD-CP-497, Paper 8, Nov. 1991.

[68]Holleman, E. C., "Summary of Flight Tests to Determine the Spin and Controllability Characteristics of a Remotely Piloted, Large-

Scale (3/8) Fighter Airplane Model," NASA TN D-8052, Jan. 1976.
[69]Iliff, K. W., Maine, R. E., and Shafer, M. F., "Subsonic Stability and Control Derivatives for an Unpowered, Remotely Piloted 3/8-Scale F-15 Airplane Model Obtained from Flight Test," NASA TN D-8136, Jan. 1976.
[70]Beyers, M. E., Huang, X. Z., Kapoor, K. B., and Peter, E., "Dynamic Stability Derivatives of a Secant-Ogive-Cylinder Configuration at High Angles of Attack," National Research Council, NAE-LTR-UA-89, Ottawa, Canada, Oct. 1987.
[71]Zan, S. J., "Measurements of Wing and Fin Buffeting on the Standard Dynamics Model," National Research Council, Inst. for Aerospace Research, NRC IAR-AN-76, Ottawa, Canada, May 1993.
[72]Guglieri, G., and Quagliotti, F. B., "Determination of Dynamic Stability Parameters in a Low Speed Wind Tunnel," AIAA Paper 91-3245, Sept. 1991.
[73]Cocquerez, J. L., Coton, P., and Verbrugge, R., "Etude de l'Effet de Sol sur Maquette en Vol," AGARD-CP-465, Paper 22, April 1990.
[74]Ericsson, L. E., "Another Look at High-Alpha Support Interference," *Journal of Aircraft*, Vol. 28, No. 5, 1991, pp. 584–591.
[75]Malcolm, G. N., "Rotary-Balance Experiments on a Modern Fighter Aircraft Configuration at High Reynolds Numbers," AIAA Paper 85-1829, Aug. 1985.
[76]O'Leary, C. O., and Weir, B., "Effect of Reynolds Number, Mach Number and Sting Geometry on Rotary Balance Measurements," International Council of the Aeronautical Sciences, ICAS Paper 90-3.8.1, Sept. 1990.
[77]O'Leary, C. O., private communication, Defence Research Agency, Bedford, England, UK, Oct. 1991.
[78]Penna, P. J., and Beyers, M. E., "Orbital Platform Concept: Flow Visualization Study of Support Interference in Rotary Experiments," National Research Council, Inst. for Aerospace Research, IAR-AN-79, Ottawa, Canada, April 1994.
[79]Ross, A. J., and Edwards, G. F., "Correlation of Predicted and Free-Flight Responses Near Departure Conditions of a High Incidence Research Model," AGARD-CP-386, Paper 31, May 1985.
[80]Tristrant, D., and Beyers, M. E., "Oscillatory Coning," AGARD-AR-265, Dec. 1990, pp. 69–76, Chap. 4.